J. Fluid Mech. (2011), *vol.* 684, *pp.* 60–84. © Cambridge University Press 2011
doi:10.1017/jfm.2011.270

An experimental study of boundary layer transition induced by a cylinder wake

A. C. Mandal† and J. Dey

Department of Aerospace Engineering, Indian Institute of Science, Bangalore-560012, India

(Received 12 August 2010; revised 14 April 2011; accepted 15 June 2011;
first published online 1 September 2011)

Boundary layer transition induced by the wake of a circular cylinder in the free stream has been investigated using the particle image velocimetry technique. Some differences between simulation and experimental studies have been reported in the literature, and these have motivated the present study. The appearance of spanwise vortices in the early stage is further confirmed here. A spanwise vortex appears to evolve into a Λ/hairpin vortex; the flow statistics also confirm such vortices. With increasing Reynolds number, based on the cylinder diameter, and with decreasing cylinder height from the plate, the physical size of these hairpin-like structures is found to decrease. Some mean flow characteristics, including the streamwise growth of the disturbance energy, in a wake-induced transition resemble those in bypass transition induced by free stream turbulence. Streamwise velocity streaks that are eventually generated in the late stage often undergo sinuous-type oscillations. Similar to other transitional flows, an inclined shear layer in the wall-normal plane is often seen to oscillate and shed vortices. The normalized shedding frequency of these vortices, estimated from the spatial spacing and the convection velocity of these vortices, is found to be independent of the Reynolds number, similar to that in ribbon-induced transition. Although the nature of free stream disturbance in a wake-induced transition and that in a bypass transition are different, the late-stage features including the flow breakdown characteristics of these two transitions appear to be similar.

Key words: boundary layer stability, transition to turbulence, vortex streets

1. Introduction

The Tollmein–Schlichting instability process during boundary layer breakdown in a quiet environment is absent in bypass transition induced by free stream turbulence (Morkovin 1969) and in wake-induced transition caused by periodically passing unsteady wakes in the free stream (Mayle 1991). The wake-induced transition scenario is often encountered in practice; for example, wakes from an upstream aerofoil in a multi-element high-lift device interact with the downstream aerofoil boundary layer; in gas turbine blades, the upstream blade wake interacts with the downstream aerofoil boundary layer, which in turn affects machine performance in terms of flow losses and heat transfer to the turbine blade (Liu & Rodi 1991). A better understanding of this process is thus important in the design of high-lift devices and in improving gas turbine performance. Broadly classified, wake–boundary layer interactions are either

† Email address for correspondence: alakesh@aero.iisc.ernet.in

https://doi.org/10.1017/jfm.2011.270 Published online by Cambridge University Press

strong or weak types (see the review by Squire 1989). The former type occurs when the initial vortex sheet persists and the two shear layers merge; a weak interaction case is when the wake is far from the boundary layer and is fully developed before it merges with the boundary layer. The study of Savill & Zhou (1983) on a flat plate boundary layer with various types of wake – such as a wake from a circular cylinder, an aerofoil, and a flat plate in the free stream – suggests interchange of vortices between the two layers and large-scale motion from the wake into the boundary layer. Zhou & Squire (1985), who studied the interaction of a single aerofoil wake with the flat plate boundary layer, propose that a potential core can exist in the initial stage of boundary layer development and a merging zone further downstream, where the main changes are confined to the inner half of the wake and the outer part of the boundary layer.

A simple representation that retains the essential physics of wake and boundary layer interactions in practical flows is the cylinder–plate combination (Ovchinnikov, Piomelli & Choudhari 2006). In order to investigate strong wake-induced transition in a flat plate boundary layer, Kyriakides *et al.* (1996) placed a circular cylinder above the plate, and upstream of the leading edge. Their experimental study revealed that transition depends on the free stream velocity, cylinder position with respect to the plate, cylinder diameter, drag coefficient and the minimum velocity in the developing wake at the streamwise position of the onset of the boundary layer transition. In their later study on the flow structure during transition (Kyriakides *et al.* 1999), they find a secondary structure of positive vorticity in the near-wall region being induced by a negative Kármán vortex in the free stream. This was based on the cross-correlation analysis of the free stream and the boundary layer measurements. Several theoretical studies (e.g. Doligalski & Walker 1984; Doligalski, Smith & Walker 1994; Pellerin & Giovannini 1999) suggest that a vortex convected above a solid wall can induce similar secondary vortex through an inviscid–viscous interaction in the form of boundary layer eruption. However, a cylinder wake generated downstream of the plate leading edge can cause boundary layer separation both upstream and downstream of the cylinder or no separation, depending on the gap between the cylinder and the plate (Price *et al.* 2002); a large-eddy simulation of this flow by Sarkar & Sarkar (2009) reveals a rapid transition to turbulence, similar to bypass transition, for a large gap between cylinder and wall.

By direct numerical simulation and large-eddy simulation, Ovchinnikov *et al.* (2006) suggest that, a short distance downstream of a cylinder placed above the leading edge, spanwise rollers that are shed from the cylinder develop spanwise-periodic deformations, which inject external wake momentum into the boundary layer. Because of this external wake momentum, streamwise velocity streaks are formed and lead to transition at higher Reynolds numbers. Interestingly, they find some features of bypass transition induced by free stream turbulence, like the distribution of u_{rms} (where u is the streamwise fluctuating velocity component) and the low-frequency spectrum of the streamwise velocity in the boundary layer even in a wake-induced transition. This is in spite of the fact that free stream disturbances are different in these two transitions. While the free stream disturbance is coherent and anisotropic in wake-induced transition, it is nearly isotropic in the case of bypass transition induced by free stream turbulence. However, in contrast to the streak spacing, of the order of the boundary layer thickness in bypass transition, Ovchinnikov *et al.* (2006) find the streak spacing, based on the deformation scale of the primary rollers, to be independent of the Reynolds numbers cases studied by them. The recent study by Pan *et al.* (2008) in a water channel suggests that a wake-induced boundary layer transition

https://doi.org/10.1017/jfm.2011.270 Published online by Cambridge University Press

is different from the low-frequency driven Klebanoff mode of transition induced by free stream turbulence. Their experimental study at a fixed Reynolds number (based on the cylinder diameter) of 2000 was based on the hydrogen bubble flow visualization technique and digital image processing of these hydrogen bubble images. Pan *et al.* (2008) find that a spanwise vortex is induced in the boundary layer due to the external Kármán wake. We may note that this feature was not reported by Ovchinnikov *et al.* (2006). Soon after the formation of a spanwise vortex, a secondary instability develops on this spanwise vortex, resulting in hairpin-like structures. Low-speed streaks that always follow a hairpin packet are generated by continuous lift-up inducement by the legs of a hairpin packet. Contrary to the observation by Ovchinnikov *et al.* (2006), Pan *et al.* (2008) do not find self-similar u_{rms} profiles. Furthermore, Pan *et al.* (2008) speculate that the peak u_{rms} movement towards the wall during transition is due to the movement of the hairpin leg towards the wall.

In view of the above-mentioned different viewpoints, further studies on the cylinder–plate combination are worth while. One such study is reported in this paper. Although Pan *et al.* (2008) measured the velocities in the wall-normal plane, the fluctuating velocity field associated with hairpin vortices and its contribution to the total u_{rms} were not reported by them. Also, the similarity, if any, in the flow randomization characteristics during transition with other transition processes is considered here. The particle image velocimetry (PIV) technique was used to measure the flow field in both the wall-normal plane and the spanwise plane over a wide Reynolds number range. The measurements being quantitative, attempts were often made to substantiate the instantaneous observations by some statistical analyses of the data.

The paper is organized as follows. The experimental details and the measurement techniques are described in § 2. The results are presented in § 3, followed by a discussion in § 4. The results are summarized in § 5.

2. Experimental details

The measurements reported here were carried out in a low-speed wind tunnel (for tunnel details, see Mandal, Venkatakrishnan & Dey 2010; Mandal 2010). A smooth circular cylinder was placed upstream and parallel to the plate leading edge to generate a Kármán wake in the free stream. Briefly, the open circuit tunnel had a contraction ratio of 14:1 and a square test section (500 mm × 500 mm × 3000 mm); the settling chamber ahead of the contraction had a smooth entry section with honeycomb and screens (four screens; 8 mesh cm^{-1}). The side-wall divergence of about 1/487 over 3 m in the test section was provided to correct for the side-wall boundary layer growth. The fan was at the end of a short diffuser, which was isolated from the rest of the tunnel to minimize the transmission of vibration. The tunnel speed, controlled by a speed controller, could reach a maximum of about 22 m s^{-1}. The free stream streamwise turbulence intensity was 0.1 % and both the cross-flow turbulent intensities were 0.05 % at 15 m s^{-1}, as measured using a cross-wire probe in two different planes. An aluminium flat plate with super-ellipse shaped leading edge (e.g. Narasimha *et al.* 1984; Narasimha & Prasad 1994) was placed horizontally in the mid-plane of the test section; the plate was 4 mm thick and 2090 mm long. The reflection of the laser sheet from the plate was reduced by sticking a smooth black sticker of 0.1 mm thickness to the plate and covering the leading edge (Banerjee, Mandal & Dey 2006; Mandal *et al.* 2010). Both the hot-wire and the PIV measurements were made in the boundary layer that developed on this smooth black surface. A schematic diagram

https://doi.org/10.1017/jfm.2011.270 Published online by Cambridge University Press

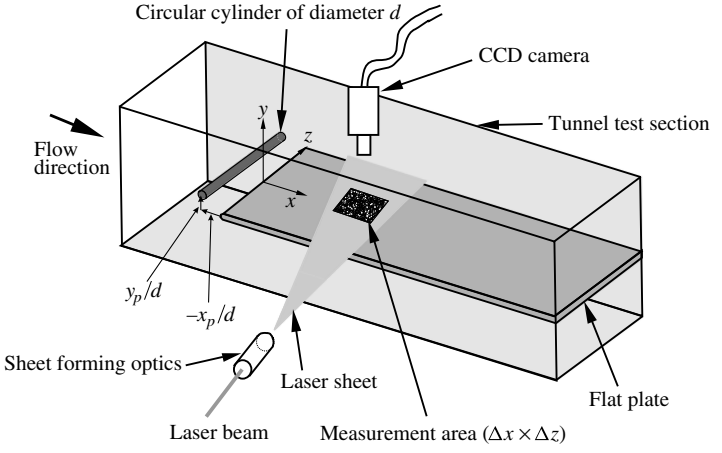


FIGURE 1. A schematic diagram of the setup and the PIV measurement zone.

of the measurement setup in the test section is shown in figure 1. The streamwise, the wall-normal and the spanwise distances are denoted by x, y and z, respectively; the plate leading edge is at $x = 0$; $z = 0$ is the plate centre-line. Two smooth circular cylinders of diameters $d = 9$ mm and 19 mm were used to generate wake in the free stream; hereafter, these two cases are designated as d_1 and d_2, respectively. In both these cases, the upstream position of the cylinder (figure 1) was fixed at $x_p/d = -1$ and the wall-normal position, y_p/d, was varied between 3 and 4. We may note that the x_p and y_p distances were measured from the tip of the super-elliptical leading edge, which was slightly below the plane surface of the flat plate. The free stream velocity is denoted by U_0, and the mean velocity by $\overline{U}$; Re_d $(=U_0 d/\nu)$ denotes the Reynolds number based on the cylinder diameter. The instantaneous velocity components in the x, y and z directions are U_I, V_I and W_I, respectively; the corresponding fluctuating components are u $(=U_I - \overline{U})$, v $(= V_I - \overline{V})$ and w $(=W_I - \overline{W})$, respectively. Two free stream velocities of $U_0 = 1.6$ and 2.7 m s^{-1} were chosen. The corresponding Re_d values were $Re_d = 929$ and 1568 for the cylinder d_1 and $Re_d = 1961$ and 3310 for the cylinder d_2. We may mention that, for $y_p/d = 5$, the boundary layer in these flows did not undergo transition in the domain of our investigation.

The wake frequency, f_0, behind a cylinder was measured using a constant-temperature hot-wire anemometer (5 μm tungsten wire and length-to-diameter ratio of ∼300); the hot-wire data were acquired at 2 kHz. The Strouhal frequencies, $f_0 d/U_0$, for the cylinder d_1 at $y_p/d = 3$ and 4 were 0.235 and 0.22, respectively; for the cylinder d_2 at $y_p/d = 3$ and 3.5, these were 0.22 and 0.21, respectively. The present Strouhal number values of 0.22 and 0.21 are comparable with the value of 0.215 for $y/d = 3.5$ given by Ovchinnikov *et al.* (2006). A slight increase seen in the Strouhal frequency at lower y_p/d values is due to the closeness of the cylinder to the wall (Angrill, Bergamaschi & Cossalter 1982).

The PIV unit (IDTpiv, USA) consisted of a double cavity Nd:YAG laser (New Wave Research), laser sheet optics, a charge-coupled device (CCD) camera (1360 × 1036 pixels) and the associated data processing software (proVISION II). The CCD camera, which was equipped with a 50 mm focal length lens, could capture five image pairs per second. A light sheet of 2 mm thickness, comparable with other studies (e.g. Kostas, Soria & Chong 2002), was used to illuminate the flow field. The processing

https://doi.org/10.1017/jfm.2011.270 Published online by Cambridge University Press

software was based on a mesh-free second-order accurate algorithm (Lourenco & Krothapalli 2000). The maximum PIV measurement zone ($\Delta x \times \Delta z$ in figure 1; $\Delta x \times \Delta y$ in the wall-normal plane) was approximately 60 mm × 46 mm. The distance of the centre of the PIV measurement zone from the leading edge is denoted by x_1. Sides of an image with lower intensity were not considered. Using an interrogation window size of 24 × 24 pixels, the acquired images were processed with a 100 × 100 rectangular mesh in the spanwise plane and 100 × 200 mesh in the wall-normal plane to cover the entire image. The limit of the interpolated vectors was set as 20 in 20 000 vectors per frame, i.e. frames showing more than 20 interpolated vectors were skipped. The spatial resolution of the measurements in terms of the correlation window size was approximately 1 mm in both the wall-normal plane and the spanwise plane; these parameters are similar to our previous studies (Banerjee *et al.* 2006; Mandal *et al.* 2010).

Blasius flow was established at $x_1 = 250$ mm with $U_0 = 1.6$ and 2.7 m s^{-1}, as shown in figure 2(*a*); the displacement thickness, δ^*, at x_1 is denoted by δ_0^*. Various quantities in the turbulent wake were measured behind the cylinder d_1, which was held parallel to the leading edge at location $x = 100$ mm and $y = 120$ mm in the free stream. The Re_d value was 929. In the absence of any data corresponding to $Re_d = 929$ in the literature, the present measurements are compared with the turbulent-wake data of Ong & Wallace (1996) at $x/d = 3$ and $Re_d = 3900$ in figure 2(*b–f*). The measured variations of the mean velocities, u_{rms} and v_{rms} and the Reynolds shear stress, $\overline{uv}$, show reasonable agreement with the data of Ong & Wallace (1996); the differences seen may be attributed to the Reynolds number effect.

3. Results

The PIV measurements presented in this section were carried out by centring the camera at $x_1 = 150$, 250 and 350 mm. The spanwise plane measurements were approximately made at the wall-normal distance y, corresponding to the peak u_{rms}, except for the $Re_d = 929$ and 1961 cases at $x_1 = 150$ mm, for which the measurement planes were at $y/\delta_0 \approx 0.1$ and 0.2, respectively.

3.1. *Spanwise structure in the boundary layer*

Some typical instantaneous PIV realizations at $x_1 = 150$ mm, for the cylinder d_2 at $y_p/d = 3$, shown in figure 3 depict the early stage of the boundary layer flow at two different Reynolds numbers. For $Re_d = 1961$, figures 3(*a*) and 3(*c*) correspond to the wall-normal plane and the spanwise plane, respectively; similarly figures 3(*b*) and 3(*d*) correspond to these two planes, respectively, for $Re_d = 3310$. Arrows in figures 3(*a*) and 3(*b*) are the instantaneous velocity vectors in the foreground of the normalized instantaneous spanwise vorticity, $\Omega_z\delta_0/U_0$, viewed by an observer moving at $0.8U_0$; arrows in figures 3(*c*) and 3(*d*) are the fluctuating velocity vectors over the instantaneous streamwise velocity contours, U_I/U_0. Spanwise vortices are seen to be the early-stage flow feature. Since negative vortices (clockwise) in the boundary layer are often accompanied by positive vortices (anticlockwise) in the free stream (see figure 3*a*,*b*), negative spanwise vortices in the boundary layer are perhaps induced by positive wake vortices in the free stream. The elongated low- and high-velocity regions in the spanwise plane (figure 3*c*) most probably correspond to the spanwise vortices in the boundary layer. Since a spanwise vortex brings comparatively high-speed fluid from the outer part of the boundary layer and pumps out low-speed fluid from the near-wall region, a cross-section in the spanwise plane will

https://doi.org/10.1017/jfm.2011.270 Published online by Cambridge University Press

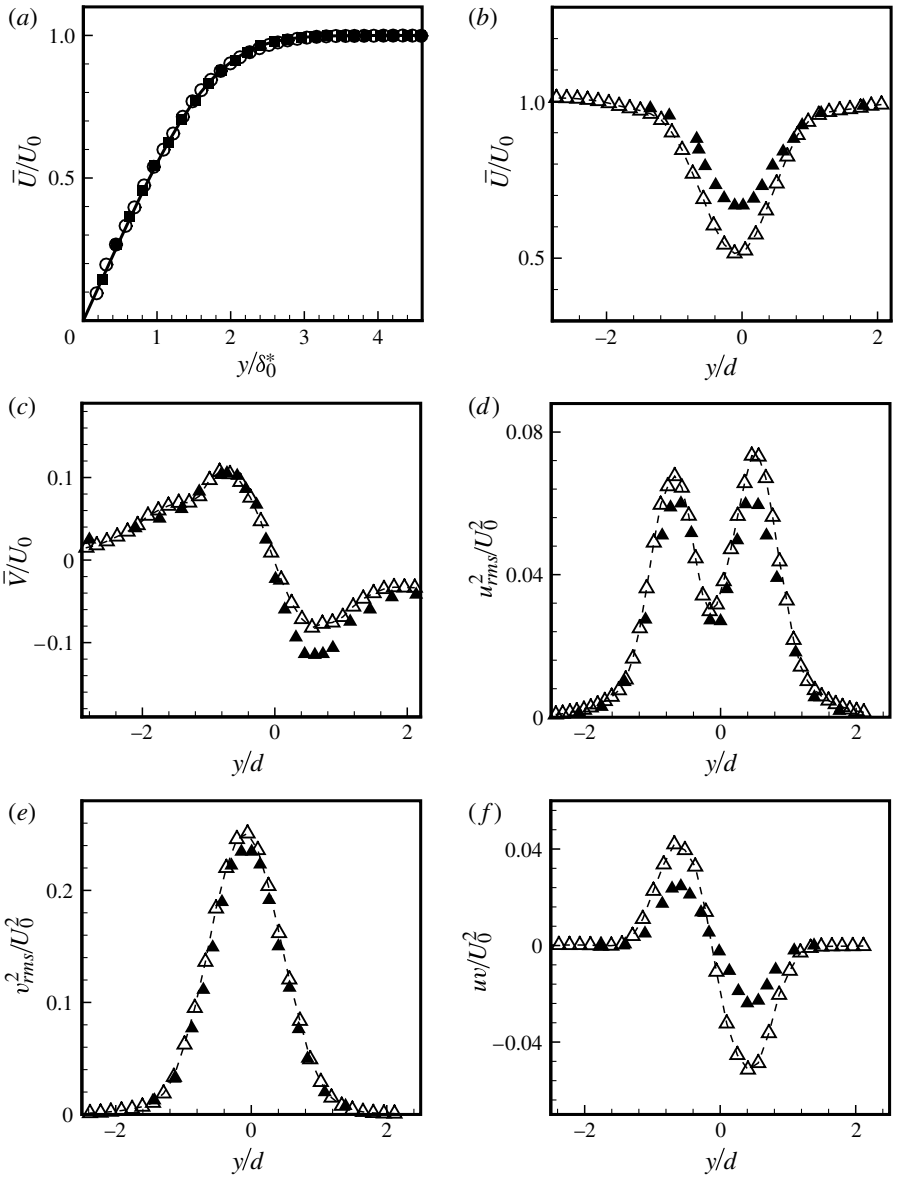


FIGURE 2. Validation of the PIV measurements. (*a*) Comparison of the measured mean velocity with the Blasius profile (—): ○, $U_0 = 1.6\ \mathrm{m\ s^{-1}}$; ■, $U_0 = 2.7\ \mathrm{m\ s^{-1}}$. (*b–f*) Comparison of various measured quantities (–△–) in the wake of the cylinder d_1 at $x/d = 3$ and $Re_d = 929$ with the data (▲) of Ong & Wallace (1996) at $x/d = 3$ and $Re_d = 3900$.

depict high- and low-velocity regions. At a higher Reynolds number of $Re_d = 3310$, Λ-shaped structures are often seen to appear in the flow, as illustrated in figure 3(*d*). Therefore, the spanwise vortex in figure 3(*b*), along with an inclined shear layer, corresponds to a Λ structure, which is often found to be associated with an inclined shear layer in the wall-normal plane (e.g. Zhou *et al.* 1999). Compared to the mean velocity, a lower instantaneous velocity inside a Λ structure and a higher velocity outside of it can be seen in figure 3(*d*). Here a Λ structure is identified from the

https://doi.org/10.1017/jfm.2011.270 Published online by Cambridge University Press

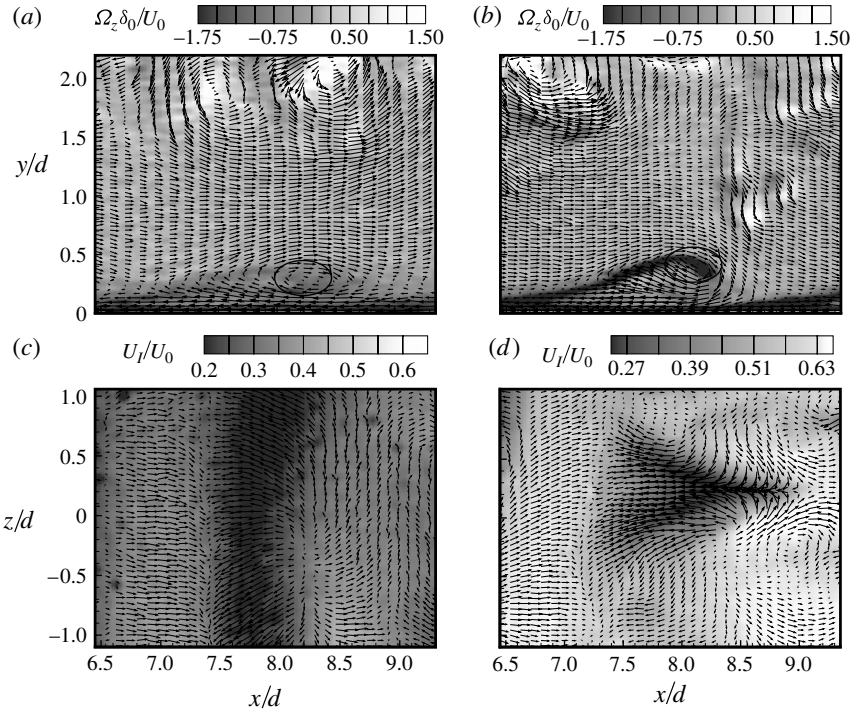


FIGURE 3. Instantaneous flow features depicting spanwise and Λ vortices, for the cylinder d_2 at $y_p/d = 3$: (*a*,*c*) for $Re_d = 1961$; and (*b*,*d*) for $Re_d = 3310$. Arrows in (*a*, *b*) are instantaneous velocity vectors in the wall-normal plane seen by an observer moving at $0.80U_0$; contours are of $\Omega_z\delta_0/U_0$. Arrows in (*c*,*d*) are the fluctuating velocity vectors of u and w in the spanwise plane over the contours of U_I/U_0.

associated Λ-type velocity field; this is not unusual in view of the similar deduction by Schröder (2001), for example, in his study of controlled boundary layer transition using stereo-particle image velocimetry (see his figures 25 and 26). Flow visualization in a water channel by Pan *et al.* (2008) also revealed the existence of spanwise vortices, which subsequently evolve into a hairpin-like structure due to the secondary instability. Figure 3(*d*) shows similar aspects, in the sense that an initial spanwise vortex is seen to evolve into a Λ structure. The present quantitative measurements thus further confirm the results of Pan *et al.* (2008). Horseshoe, Λ, omega-shaped vortices and their deformed versions, being variations of a common basic flow structure at different stages of evolution, are often recognized as hairpin vortices (e.g. Adrian, Meinhart & Tomkins 2000; Pan *et al.* 2008), as is also considered here.

The physical size of these downstream evolving vortices depends on the Reynolds number and the upstream cylinder position. As an example, a bigger Λ can be seen in figure 4(*a*) for the $y_p/d = 3$ and $Re_d = 1961$ case, compared to the $y_p/d = 3$ and $Re_d = 3310$ case in figure 3(*d*); similarly, when the cylinder position is raised to $y_p/d = 3.5$, a larger Λ structure appears at the same $Re_d = 3310$ (figure 4*b*). Sometimes streaks are also seen to accompany these Λ vortices (for example, see the $z/d \leqslant -1$ region in figure 4*a*). Furthermore, the staggered pattern of hairpin vortices, as in figure 4(*b*), was often found in several PIV realizations. Corresponding to the flows in figures 3(*a*) and 4(*a*), the power spectra (of the hot-wire signal in

https://doi.org/10.1017/jfm.2011.270 Published online by Cambridge University Press

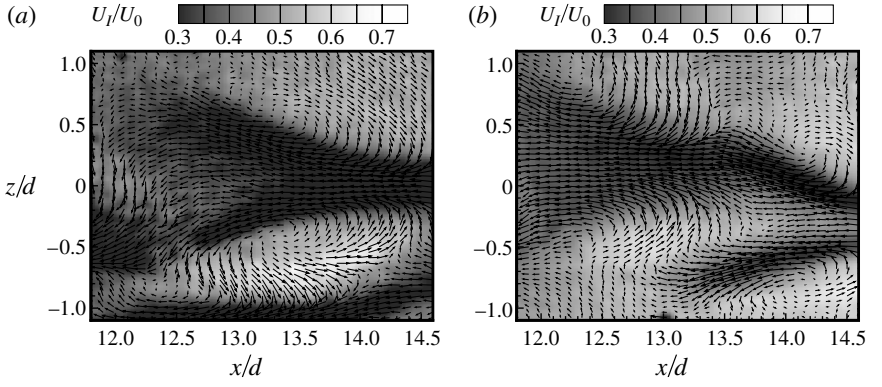


FIGURE 4. Larger Λ structures at $x_1 = 250$ mm: (*a*) $y_p/d = 3$ and $Re_d = 1961$; and (*b*) $y_p/d = 3.5$ and $Re_d = 3310$. Fluctuations of u and w are shown as vectors over U_I/U_0 contours.

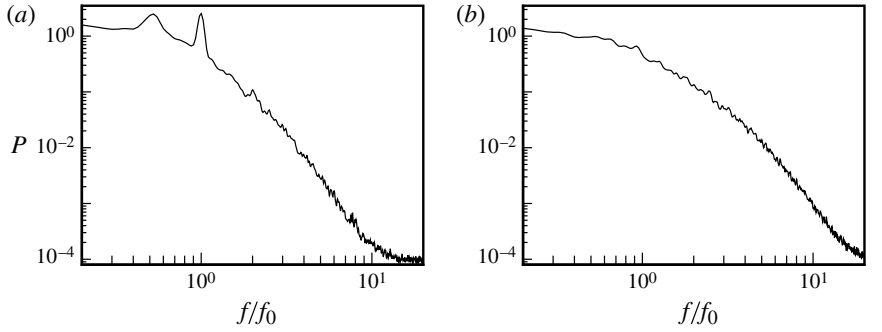


FIGURE 5. Power spectra of hot-wire traces at $y/\delta_0 \approx 0.4$ in the boundary layer for the cylinder d_2 at $y_p/d = 3$ and $Re_d = 1961$: (*a*) spectrum at $x_1 = 150$ mm; and (*b*) spectrum at $x_1 = 250$ mm.

the boundary layer) are displayed in figures 5(*a*) and 5(*b*), respectively; P denotes the power in an arbitrary scale, and the frequency, f, is normalized by the wake Strouhal frequency, f_0. The peak at the shedding frequency of the cylinder, along with a small harmonic peak and a slightly broad-band quasi-subharmonic peak (figure 5*a*), which diminishes downstream (figure 5*b*), are similar to the results reported by others (e.g. Kyriakides *et al.* 1996; Ovchinnikov *et al.* 2006; Pan *et al.* 2008). Ovchinnikov *et al.* (2006) suggest that the peak at the Strouhal frequency is due to the instant propagation of wake unsteadiness through pressure. On the other hand, Pan *et al.* (2008) attribute this ($f/f_0 = 1$) to the periodic generation of secondary transverse vortices, which is seen to be so here, as well (figure 3*a*,*c*). Figure 3(*d*) clearly shows that the evolution of Λ vortices from a two-dimensional spanwise vortex is a major sequence in a wake-induced transition. These Λ vortices appear in a staggered pattern (figure 4), similar to those seen in other boundary layer transitions (see, for example, Gad-el-Hak *et al.* 1984; Bake, Fernholz & Kachanov 2000; Liu, Zaki & Durbin 2008), although the generation process is different in all these cases. The staggered pattern of Λ vortices in figure 4 at $x_1 = 250$ mm may therefore be traced back to the subharmonic disturbance seen in the spectrum at $x_1 = 150$ mm (figure 5*a*).

https://doi.org/10.1017/jfm.2011.270 Published online by Cambridge University Press

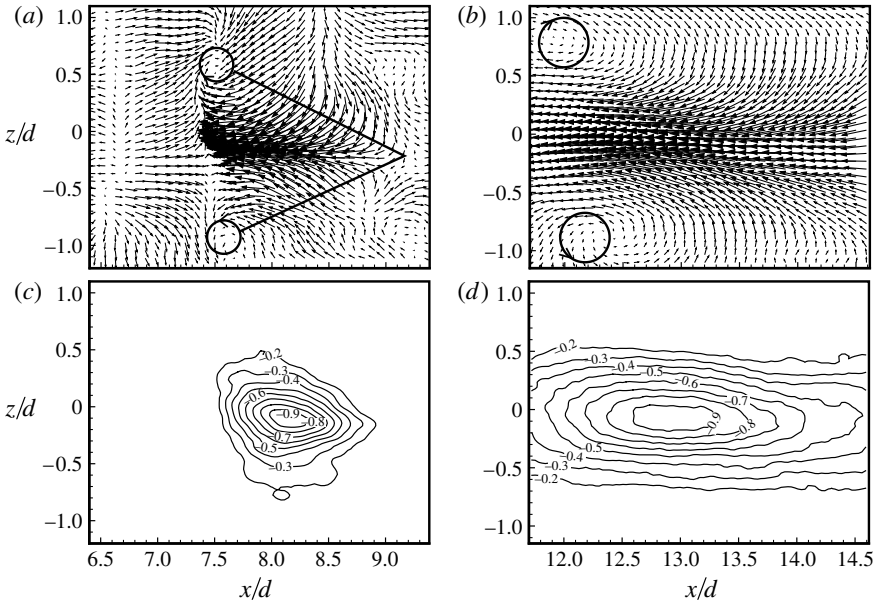


FIGURE 6. Conditional flow structures in the spanwise plane given a negative u velocity event, for the cylinder d_2 at $y_p/d = 3$. (*a*,*b*) In terms of fluctuating velocity vectors at $x_1 = 150$ mm ($Re_d = 3310$) and $x_1 = 250$ mm ($Re_d = 1961$), respectively. (*c*,*d*) Only for u velocity component, for flows in (*a*,*b*), respectively.

The Λ/hairpin vortices discussed above are the common flow feature in wake-induced transition in boundary layers. Therefore, if such flow features are consistent with the majority of PIV realizations, their signature should also be evident in the flow statistics. As a hairpin vortex accumulates low-velocity fluid inside it by its counter-rotating legs, a conditional average structure may be sought with a given negative u velocity event. The estimate is expressed as $\langle \boldsymbol{v}(\boldsymbol{x}')|u(\boldsymbol{x})\rangle$, where $\boldsymbol{v} = (u, w)$ and $\boldsymbol{x} = (x, z)$. Because direct computation of this conditional average is difficult, a linear stochastic estimate can provide the conditional average of a process with unconditional data (Adrian 2007; Christensen & Adrian 2001). We estimated the conditional average of the fluctuating velocity field following Tomkins & Adrian (2003), with a given negative u velocity event,

$$\langle v_j(\boldsymbol{x}')|u(\boldsymbol{x})\rangle \approx A_j u(\boldsymbol{x}). \tag{3.1}$$

Here, the kernel A_j is determined by minimizing the mean-square error of the estimate, which yields

$$\langle v_j(\boldsymbol{x}')|u(\boldsymbol{x})\rangle \approx \frac{\langle u(\boldsymbol{x})v_j(\boldsymbol{x}')\rangle}{\langle u(\boldsymbol{x})u(\boldsymbol{x})\rangle}u(\boldsymbol{x}). \tag{3.2}$$

Thus an estimate of the conditional average can be approximated by the unconditional two-point correlation, and the fluctuating velocity behaviour on an average basis can be obtained with a given negative $u(\boldsymbol{x})$. The conditional structures so obtained for the flows in figures 3(*d*) and 4(*a*) are shown in figure 6. We used 296 PIV realizations, whereas Tomkins & Adrian (2003) used 201 realizations in a similar analysis. In terms of the fluctuating velocity vectors of u and w, the hairpin signature, that is, a strong negative velocity region, along with two counter-rotating vortices in figure 6(*a*,*b*),

https://doi.org/10.1017/jfm.2011.270 Published online by Cambridge University Press

Cylinder	x_p/d	y_p/d	Re_d	x_1 (mm)	δ_0 (mm)	δ_0^* (mm)	H	Re_θ	S_n
d_1	−1	3.0	929	150	9.4	2.35	2.02	120	400
d_1	−1	3.0	929	250	14.0	2.39	1.94	127	488
d_1	−1	3.0	1568	150	8.0	1.73	1.92	157	309
d_1	−1	3.0	1568	250	10.5	1.69	1.82	162	408
d_1	−1	4.0	1568	150	5.7	2.02	2.64	133	359
d_1	−1	4.0	1568	250	8.4	2.32	2.19	185	407
d_1	−1	4.0	1568	350	10.0	2.64	2.06	223	212
d_2	−1	3.0	1961	150	7.0	2.50	2.53	102	400
d_2	−1	3.0	1961	250	12.5	2.80	2.00	143	300
d_2	−1	3.0	3310	150	8.5	1.88	2.11	155	323
d_2	−1	3.5	3310	150	5.7	2.08	2.60	139	399
d_2	−1	3.5	3310	350	9.5	2.62	2.26	202	329

TABLE 1. Different flow cases and the boundary layer parameters at x_1.

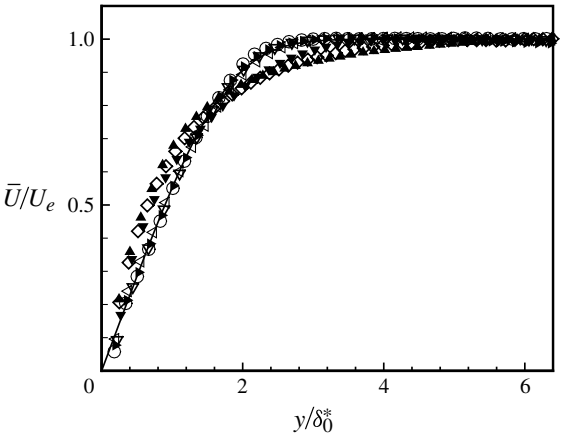


FIGURE 7. Comparison of the mean velocity profiles with the Blasius profile (—). Case d_1 and $Re_d = 929$: ▶, $x/d = 16.6$ ($y_p/d = 4$); ▲, $x/d = 27.7$ ($y_p/d = 3$). Case d_1 and $Re_d = 1568$: ▽, $x/d = 16.6$ ($y_p/d = 4$); ▼, $x/d = 27.7$ ($y_p/d = 4$). Case d_2 and $Re_d = 1961$: ◁, $x/d = 7.9$ ($y_p/d = 3$); ◇, $x/d = 13.2$ ($y_p/d = 3$); ○, $x/d = 7.9$ ($y_p/d = 4$).

is similar to that of Tomkins & Adrian (2003) in a turbulent boundary layer flow. Figures 6(*c*) and 6(*d*), based on a single velocity component, u, show a reduced length scale at a higher Re_d, for the same $y_p/d = 3$, as was also observed in our instantaneous PIV realizations.

3.2. *Mean flow*

The boundary layer integral parameters in table 1 are based on the effective free stream velocity, U_e, which, following Ovchinnikov *et al.* (2006), is the maximum free stream velocity between the wake and the wall. Here S_n is the number of PIV realizations used in ensemble averaging. The boundary layer thickness, δ, corresponds to $0.99U_e$, and its value at the measurement location x_1 is denoted by δ_0; the shape factor (δ_0^*/θ) is denoted by H, where θ is the momentum thickness at x_1.

Figure 7 shows a comparison of the measured mean velocity profiles in the boundary layer for different flows with the Blasius profile. The instantaneous PIV

https://doi.org/10.1017/jfm.2011.270 Published online by Cambridge University Press

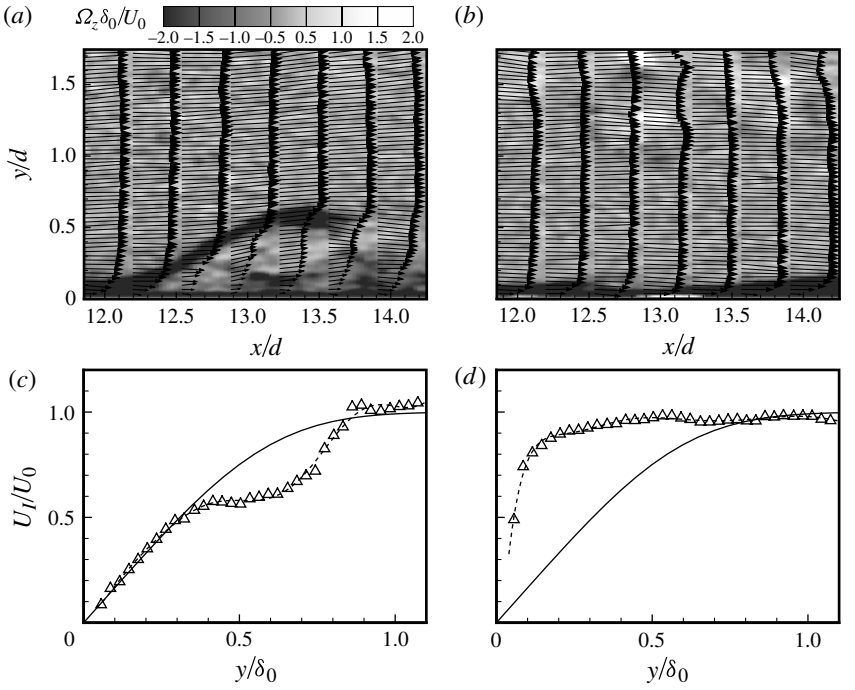


FIGURE 8. (*a*,*b*) Instantaneous PIV realizations at $x_1 = 250$ mm depicting typical inflectional and fuller velocity profiles, respectively. Cylinder d_2 at $y_p/d = 3$ and $Re_d = 1961$. Arrows are instantaneous velocity vectors over the contours of $\Omega_z\delta_0/U_0$. (*c*,*d*) Comparison of the instantaneous velocity profiles (△) at about $x/d \approx 13$ in (*a*, *b*) with the Blasius profile (—), respectively.

realizations at $x_1 = 150$ mm showed spanwise vortices for the flow parameters: $y_p/d = 4$, $Re_d = 1568$, for the cylinder d_1; and $y_p/d = 3$, $Re_d = 1961$, for cylinder d_2. However, no such spanwise vortex was seen for $y_p/d = 4$ and $Re_d = 929$ (for d_1) and 1961 (for d_2) cases. Figure 7 shows that the presence of a spanwise vortex does not significantly distort the mean velocity profiles at $x_1 = 150$ mm from the Blasius one. Also, the velocity profiles in the presence of hairpin vortices and streaks at $x_1 = 250$ mm are independent of the cylinder size, and resemble those in bypass transition induced by free stream turbulence (see, for example, Westin *et al.* 1994; Matsubara & Alfredsson 2001) in the sense that there is a velocity gain in the inner part of the boundary layer and a deficit in the outer part. The measured profile shapes are similar to those simulated by Ovchinnikov *et al.* (2006), who, however, do not report any spanwise vortex. Pan *et al.* (2008) find only velocity deficit, irrespective of the spanwise vortex near the leading edge. They also suggest that a secondary transverse vortex contributes to the mean velocity deficit inside the boundary layer due to the eruption of low-speed fluid. However, a spanwise vortex in the boundary layer not only ejects low-speed fluid from the wall region to the outer part of the boundary layer but also brings in high-speed fluid from the outer part of the boundary layer to the near-wall region. Here we find that mainly two types of instantaneous velocity fields, as shown in figure 8(*a*,*b*), for $y_p/d = 3$ and $Re_d = 1961$ (same flow as in figure 4*a*), contribute to the velocity deficit and gain, respectively. Arrows in this figure are instantaneous velocity vectors over the contours of normalized instantaneous

https://doi.org/10.1017/jfm.2011.270 Published online by Cambridge University Press

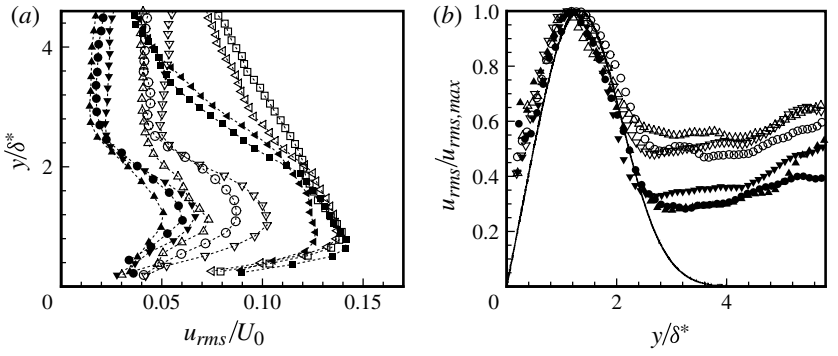


FIGURE 9. (*a*) Distribution and (*b*) self-similarity of u_{rms} profiles across the boundary layer for cylinder d_2 (open symbols, $y_p/d = 3$ and $Re_d = 1961$) and cylinder d_1 (filled symbols, $y_p/d = 4$ and $Re_d = 1568$): △, $x/d = 6.5$; ○, $x/d = 8.3$; ▽, $x/d = 9.4$; ◁, $x/d = 12.5$; □, $x/d = 13.4$; ▲, $x/d = 14$; ●, $x/d = 16.6$; ▼, $x/d = 19.5$; ◀, $x/d = 27.5$; ■, $x/d = 40$. The full curve in (*b*) is from Luchini (2000).

spanwise vorticity, $\Omega_z\delta_0/U_0$. Figure 8(*a*) shows highly inflectional velocity profiles, along with an inclined shear layer. This is better seen in figure 8(*c*), where the present data at $x/d \approx 13$ are compared with the Blasius profile. Similarly, figures 8(*b*) and 8(*d*) show fuller velocity profiles. Manifestation of these low- and high-velocity regions, compared to the mean velocity, may be attributed to hairpin vortices, which pump low-velocity fluid inside and bring high-velocity fluid from outside, as mentioned in the previous section.

The measured u_{rms} profiles in the boundary layers at various streamwise locations are shown in figure 9(*a*); for the cylinder d_1, $y_p/d = 4$ and $Re_d = 1568$; and for the cylinder d_2, $y_p/d = 3$ and $Re_d = 1961$. During the initial growth phase, the peak in the u_{rms} profiles occurs at about $y/\delta^* \approx 1.2$, and it moves towards the wall at downstream locations. These compare well with other studies (e.g. Ovchinnikov *et al.* 2006; Pan *et al.* 2008). The u_{rms} peak at $y/\delta^* \approx 1.2$ is close to $y/\delta^* \approx 1.3$ in bypass transition induced by free stream turbulence (e.g. Westin *et al.* 1994; Matsubara & Alfredsson 2001). In the early growth stage, near self-similarity of u_{rms} that closely follows the non-modal distribution of Luchini (2000) is shown in figure 9(*b*), where $u_{rms}/u_{rms,max}$ is plotted against y/δ^*; data in this figure correspond to those for $x/d < 20$, for d_1, and to $x/d < 10$, for d_2, in figure 9(*a*). This self-similarity is in agreement with Ovchinnikov *et al.* (2006), but differs from the finding of Pan *et al.* (2008); the reason for this difference may be due to the fact that Pan *et al.* (2008) used hydrogen bubbles as seeding particles rather than the conventional seeding particles for PIV measurements.

The measured streamwise growth of the disturbance energy is compared with other previous studies in figure 10(*a*). We may note that the present y_p/d is not exactly the same as y/d (distance from the plate surface) considered by other investigators. It can be seen that a small initial slow growth region is followed by a rapid linear growth of the disturbance energy. Compared to the lower growth rate reported by Pan *et al.* (2008), the present measurements show a similar energy growth rate as simulated by Ovchinnikov *et al.* (2006). Also, one can see a close agreement between the present case of $Re_d = 1961$ and $y_p/d = 3$ with the $Re_d = 1155$ and $y/d = 3.5$ case of Ovchinnikov *et al.* (2006). However, the results of Pan *et al.* (2008), although showing nearly linear energy growth, are different. In bypass transition induced by free stream

https://doi.org/10.1017/jfm.2011.270 Published online by Cambridge University Press

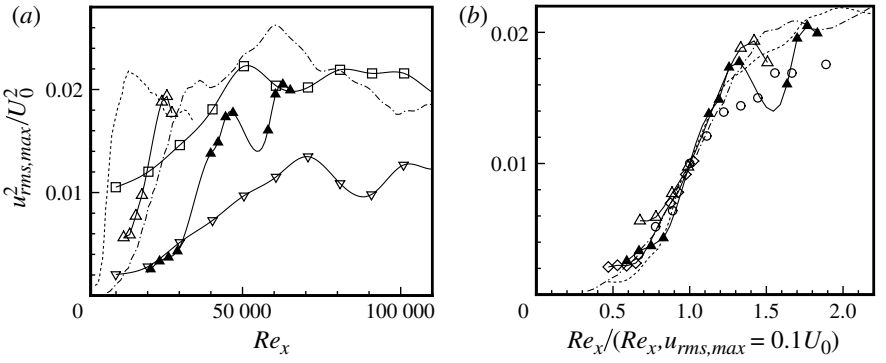


FIGURE 10. (*a*) Streamwise growth and (*b*) rescaled streamwise growth of the peak disturbance energy, $u^2_{rms,max}/U_0^2$. Ovchinnikov *et al.* (2006): · · · · ·, $Re_d = 385$ and $y/d = 3.5$; – · – · –, $Re_d = 1155$ and $y/d = 3.5$. Pan *et al.* (2008): –□–, $Re_d = 2000$ and $y/d = 3.25$; –▽–, $Re_d = 2000$ and $y/d = 4$. Present: –△–, $Re_d = 1961$ and $y_p/d = 3$ (cylinder d_2); –▲–, $Re_d = 1568$ and $y_p/d = 4$ (cylinder d_1). The data of Pan *et al.* (2008) are not shown in (*b*). (Re_x, $u_{rms,max} = 0.1U_0$) is the Re_x value corresponding to $u_{rms,max} = 0.1U_0$. Data of Kyriakides *et al.* (1996) (○, $y/d = 2.5$ and $Re_d = 3500$) and present study (◇, cylinder d_2 at $y_p/d = 3.5$ and $Re_d = 1961$) are also shown in (*b*).

turbulence, the distance over which the discrepant free stream and boundary layer length scales adjust may correspond to the initial slow energy growth region (Fransson, Matsubara & Alfredsson 2005; Ovchinnikov, Choudhari & Piomelli 2008). In the case of wake-induced transition, however, the slow initial growth region may correspond to the onset of the spanwise vortex in the boundary layer. Interestingly, we find that, except for the data of Pan *et al.* (2008), the other data in the rapidly growing linear stage in figure 10(*a*) collapse when, following Fransson *et al.* (2005), the streamwise Reynolds number, Re_x, is scaled with the Re_x value corresponding to $u_{rms,max} = 0.1U_0$. This is elucidated in figure 10(*b*), where the data from Kyriakides *et al.* (1996) are also displayed. In terms of this scale, Fransson *et al.* (2005) find the linear growth of $u_{rms,max}$ for a wide range of free stream turbulence intensity; however, the growth rate in figure 10(*b*) is steeper than that reported by Fransson *et al.* (2005) (see their figure 10*b*). Therefore, it seems that only the initial slow growth of the disturbance is influenced by the cylinder diameter and its upstream position in wake-induced transitions. Also, the near non-modal distribution of the u_{rms} profiles and the rapid linear growth stage suggest that, at some stage of the disturbance development (most likely while a spanwise vortex deforms to create hairpin structures and streaks), even a wake-induced transition may undergo algebraic growth.

3.2.1. *Conditional* u_{rms}

On an average basis, u_{rms} is a measure of fluctuation amplitude in a perturbed boundary layer. Nonetheless, simultaneous fluctuations over a spatial domain may also reveal some coherent patterns of these fluctuations, which are of interest in understanding the flow (e.g. Jacobs & Durbin 2001). Corresponding to the instantaneous realizations at $x_1 = 250$ mm shown in figure 8(*a*,*b*), the velocity fluctuations are displayed (by vectors of u and v) in figures 11(*a*) and 11(*b*), respectively, over $\Omega_z\delta_0/U_0$ contours. Figure 11(*a*) depicts negative u fluctuations in the inclined shear layer, while figure 11(*b*) shows positive u fluctuations in the high-shear layer near the wall. These are typical fluctuations in wake-induced transition cases

https://doi.org/10.1017/jfm.2011.270 Published online by Cambridge University Press

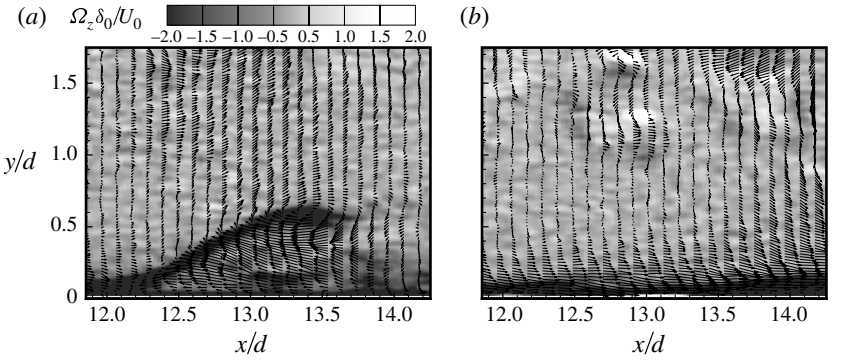


FIGURE 11. Typical instantaneous (*a*) negative u fluctuations in the lifted-up shear and (*b*) positive u fluctuations near the wall in the wall-normal plane. Cylinder d_2 at $y_p/d = 3$, $x_1 = 250$ mm and $Re_d = 1961$. Grey levels: normalized instantaneous vorticity. Arrows: fluctuating velocity vectors.

reported here. Interestingly, these features are also seen in bypass transition induced by free stream turbulence (Jacobs & Durbin 2001; Mandal *et al.* 2010). We may also mention that a hairpin vortex is associated with an inclined shear layer and negative streamwise velocity fluctuations (e.g. Zhou *et al.* 1999; Bake *et al.* 2000).

While transition progresses in the downstream direction, the peak of u_{rms} moves towards the wall, as shown in figure 9(*a*). Pan *et al.* (2008) speculate that this shift is due to the wall-ward movement of the hairpin leg and suggest further studies in this regard. In order to assess the individual contributions of positive and negative fluctuations to the total u_{rms}, we separated these fluctuations by conditional sampling (Mandal *et al.* 2010), as follows. In each PIV realization, data points showing positive and negative u fluctuations and their magnitude at those points were found first. We then used the magnitude and the sign criteria to pick up a particular u fluctuation. For either positive or negative u fluctuation, if the magnitude of that u fluctuation exceeded 5 % of the free stream velocity at large numbers of data points than other u fluctuations, it was considered for processing. For example, a positive u fluctuation showing $u/U_0 \geqslant 5\,\%$ over 20–30 % of the total data points and smaller fluctuations at other data points in the same PIV realization were considered. We may note that the free stream fluctuation due to the wake was excluded by considering the wall-normal extent of about $(6\text{–}7)\delta^*$. Denoting the r.m.s. of positive u fluctuations by $u_{rms,p}$, and negative u fluctuations by $u_{rms,n}$, their distributions for both the cylinders at $y_p/d = 3$ are shown in figure 12(*a*,*b*), for $Re_d = 1961$ and 929, respectively. It can be seen that the $u_{rms,p}$ peak is more towards the wall, whereas the $u_{rms,n}$ peak is away from the wall, as in bypass transition induced by free stream turbulence; two peaks in the $u_{rms,n}$ profile could be due to the prevalence of hairpin structures (e.g. Acarlar & Smith 1987). A linear combination (Mandal *et al.* 2010) of $u_{rms,p}$ and $u_{rms,n}$, i.e. $u_{rms,a} \approx 0.44(u_{rms,p} + u_{rms,n})$, shown in the inset in figure 12, can closely represent the total u_{rms} profile. Therefore, the wall-ward movement of the u_{rms} peak could be attributed to positive u fluctuations associated with the high-velocity region near the wall.

3.3. *Boundary layer streaks*

Boundary layer streaks are important coherent structures in bypass transition induced by free stream turbulence. Simulation by Ovchinnikov *et al.* (2006) also show

https://doi.org/10.1017/jfm.2011.270 Published online by Cambridge University Press

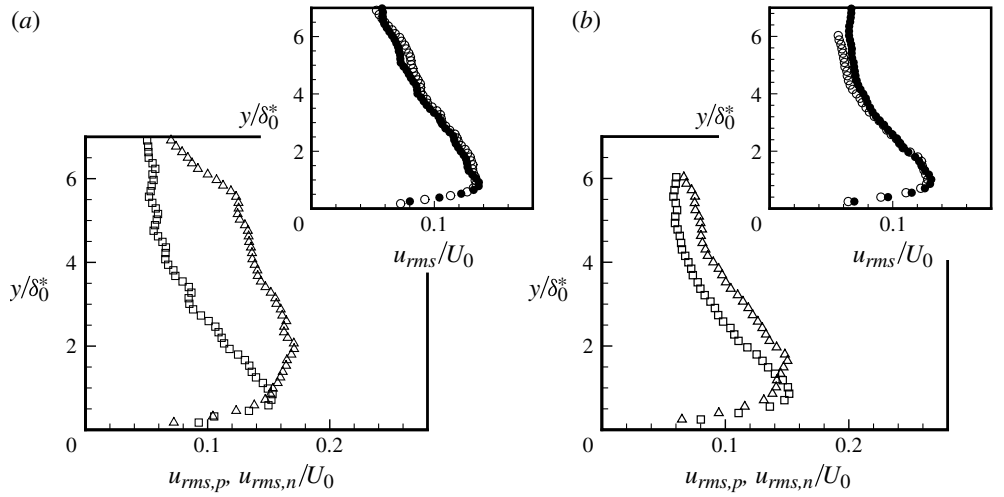


FIGURE 12. Average and conditional r.m.s. profiles associated with positive and negative u fluctuations at $x_1 = 250$ mm. Symbols: □, $u_{rms,p}$; △, $u_{rms,n}$; ○, $u_{rms,a}$; ●, u_{rms}. (*a*) Cylinder d_2; $y_p/d = 3$ and $Re_d = 1961$ case. (*b*) Cylinder d_1; $y_p/d = 3$ and $Re_d = 929$ case.

boundary layer streaks in wake-induced transition. Typical instantaneous low- and high-velocity streaks shown in figure 13(*a–d*), for both the cylinders at $y_p/d = 3$, further confirm this; fluctuating velocity vectors of u and w are shown over the contours of U_I/U_0. The fluctuation pattern of small w and large u is typical of that in bypass transition (e.g. Jacobs & Durbin 2001; Mandal *et al.* 2010). We also find that there are some triangular-shaped low-velocity regions connected to each other (figure 13*b*). Since the upstream flow is populated with hairpin vortices (see $y_p/d = 3$ and $Re_d = 3310$ case, for example), it may be expected that these low-velocity streaks have arisen due to the mean shear stretching and due to the upwelling of low-speed fluid by the legs of hairpin vortices. Also, compared to the varicose-type streak oscillation reported by Pan *et al.* (2008) from their flow visualizations, the present low-speed streaks often show sinuous-type oscillation, as illustrated in figure 13(*c*,*d*), for the cylinder d_1. Similar sinuous oscillations of low-speed streaks are also observed in other transitional flows (e.g. Swearingen & Blackwelder 1987; Konishi & Asai 2010). The streamwise wavelength of these oscillations varied approximately to within $(10–15)\delta_0^*$, in close agreement with that in bypass transition (e.g. Schlatter *et al.* 2008). We may mention that streaks were seen to appear at $x_1 = 150$ mm, for the cylinder d_1 at $y_p/d = 3$ and $Re_d = 929$, compared to the d_2 case. This is perhaps due to the fact that, because the physical distance of the cylinder d_1 above the leading edge is shorter, a Kármán wake starts interacting with the boundary layer upstream of $x_1 = 150$ mm with eventual formation of streaks at $x_1 = 150$ mm.

Streaks were found to appear randomly within the measurement window in the spanwise plane and their average spacing was estimated using the spatial correlation function (e.g. Jacobs & Durbin 2001), R_{uu} $(=\overline{u(z)u(z+dz)}/\overline{u^2(z)})$, as shown in figure 14. The spanwise distance is normalized by the cylinder diameter, d, and by the boundary layer thickness, δ_0, in figures 14(*a*) and 14(*b*), respectively. The distance between the origin and the point of minimum of R_{uu} in figure 14(*a*,*b*) is taken as half the dominating spanwise wavelength of high- and low-speed streaks. The streak spacing so obtained is approximately $2.2d$ for $Re_d = 929$, and it reduces with

https://doi.org/10.1017/jfm.2011.270 Published online by Cambridge University Press

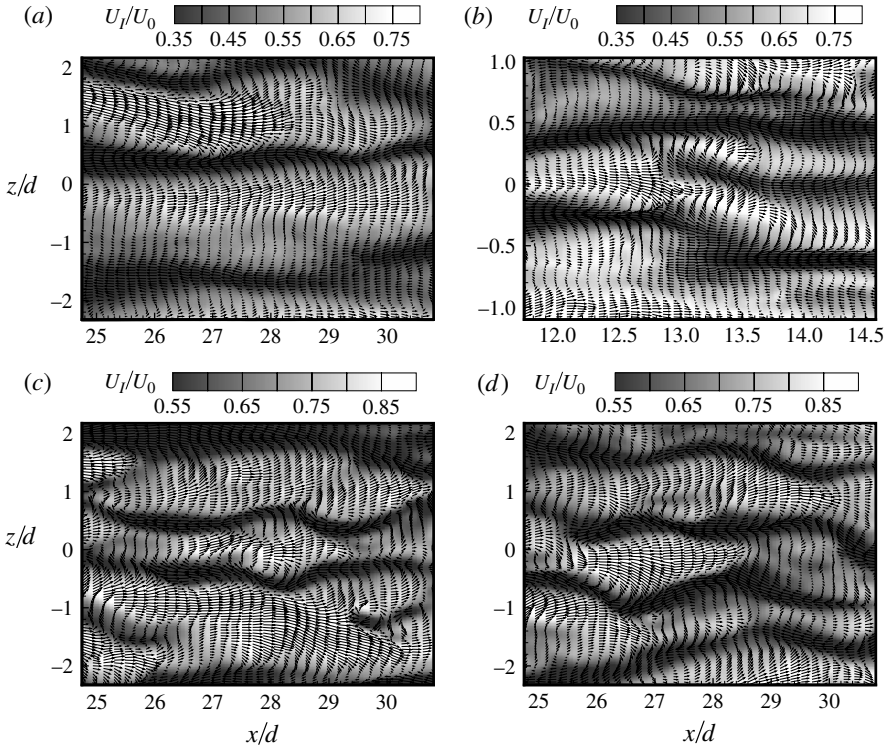


FIGURE 13. Instantaneous streamwise velocity streaks at $x_1 = 250$ mm for $y_p/d = 3$. Arrows: fluctuating velocity vectors. Grey levels: normalized instantaneous velocity. (*a*) Cylinder d_1 and $Re_d = 929$; (*b*) cylinder d_2 and $Re_d = 3310$; (*c*,*d*) cylinder d_1 and $Re_d = 1568$.

increasing Re_d. This is in agreement with Ovchinnikov *et al.* (2006), who find the average streak spacing to be $\sim 2.5d$, and it drops while turbulence sets in. In terms of the local boundary layer thickness, δ_0, the streak spacing is within $(1–3)\delta_0$ (figure 14*b*), somewhat similar to that in bypass transition (e.g. Matsubara & Alfredsson 2001).

Although streaks can be generated by various means, their breakdown may not be too sensitive to the means of their generation (Elofsson & Alfredsson 1998). In a streaky boundary layer, secondary instability of a streak has often been suggested as a route to turbulence in several studies (e.g. Swearingen & Blackwelder 1987; Andersson *et al.* 2001; Mans, de Lange & van Steenhoven 2007; Schlatter *et al.* 2008). Since the streak amplitude (based on the difference of maximum and minimum velocities) is important in the secondary disturbance growth on streaks, we consider the streak amplitude, following Andersson *et al.* (2001), as,

$$A = \tfrac{1}{2}[\max_{z,S_n}(U_I - \overline{U}) - \min_{z,S_n}(U_I - \overline{U})]. \tag{3.3}$$

Figure 15 shows the streak amplitude, $A \times 100/U_0$, for $y_p/d = 3$ and $Re_d = 929$, 1568, 3310 and 6129 cases. We may note that, for the cylinder d_2, the $Re_d = 6129$ case (at $x_1 = 350$ mm) was nearly turbulent (shape factor, $H = 1.53$). With an initial streak amplitude of $\sim 43\,\%$ of the free stream velocity, the streak amplitude can be seen to saturate at $\sim 35\,\%$ of the free stream velocity, for both the cylinders. Since the secondary instability of the streak begins at such a level of streak amplitude (e.g. Elofsson, Kawakami & Alfredsson 1999; Andersson *et al.* 2001), a similar instability

https://doi.org/10.1017/jfm.2011.270 Published online by Cambridge University Press

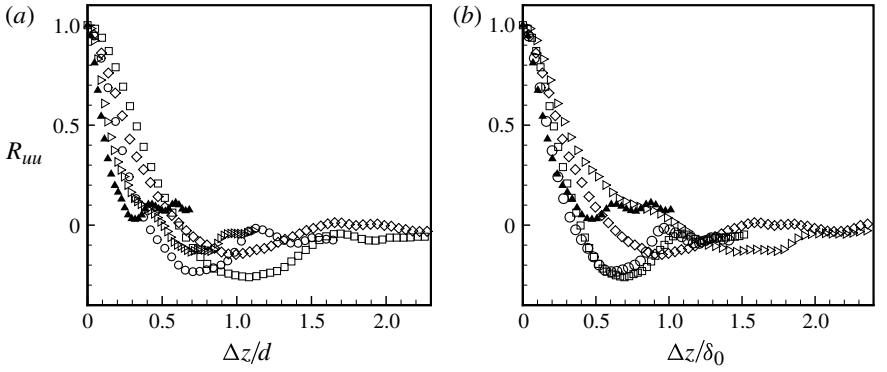


FIGURE 14. Spanwise correlation function, R_{uu}, for different Re_d, and $y_p/d = 3$. Spanwise distance is normalized by the cylinder diameter in (a) and by the boundary layer thickness in (b). Cylinder d_1: $\diamond$, $x_1 = 150$ mm and $Re_d = 929$; $\square$, $x_1 = 250$ mm and $Re_d = 929$; $\bullet$, $x_1 = 250$ mm and $Re_d = 1568$. Cylinder d_2: $\triangleright$, $x_1 = 250$ mm and $Re_d = 3310$; $\blacktriangle$, $x_1 = 350$ mm and $Re_d = 6129$.

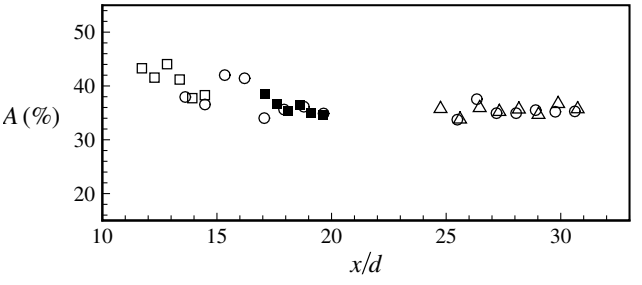


FIGURE 15. Streamwise variation of streak amplitude for different Reynolds numbers. Cylinder d_1: $\triangle$, $Re_d = 929$; $\circ$, $Re_d = 1568$. Cylinder d_2: $\square$, $Re_d = 3310$; $\blacksquare$, $Re_d = 6129$. Here $y_p/d = 3$ for all the data.

mechanism may also exist in even wake-induced boundary layer transition. A careful examination of the PIV realizations in the spanwise plane revealed some sinuous oscillations of low-speed streaks, which show a growing tendency in space; all streaks need not show this feature because of nonlinear saturation. One such low-speed streak is shown in the marked region in figure 16(a), and its zoomed view in figure 16(b), respectively; the contour line in figure 16(b) corresponds to $U_I/U_0 = 0.46$. Streamwise growth and staggered array of vortices in the sides of the low-speed streak are clearly visible; vortices, identified by the swirling strength, λ_{ci} (imaginary part of the complex eigenvalue of the local velocity gradient tensor), following Zhou *et al.* (1999), are shown by the line contours in figure 16(a). The flow simulation in the presence of streaks by Brandt & Henningson (2002) shows a staggered pattern of quasi-streamwise vortices on the flanks of sinuous low-speed streaks, both inclined away from the wall and tilted in the downstream direction. Vortices in figures 16(a) may be the cross-sections of such inclined and tilted quasi-streamwise vortices. The recent PIV measurements of controlled subharmonic sinuous streaks in the boundary layer by Konishi & Asai (2010) also reveal similar quasi-streamwise vortices in the flanks of exponentially growing sinuous low-speed streaks. They also find that these quasi-streamwise vortices developing along the neighbouring low-speed streaks

https://doi.org/10.1017/jfm.2011.270 Published online by Cambridge University Press

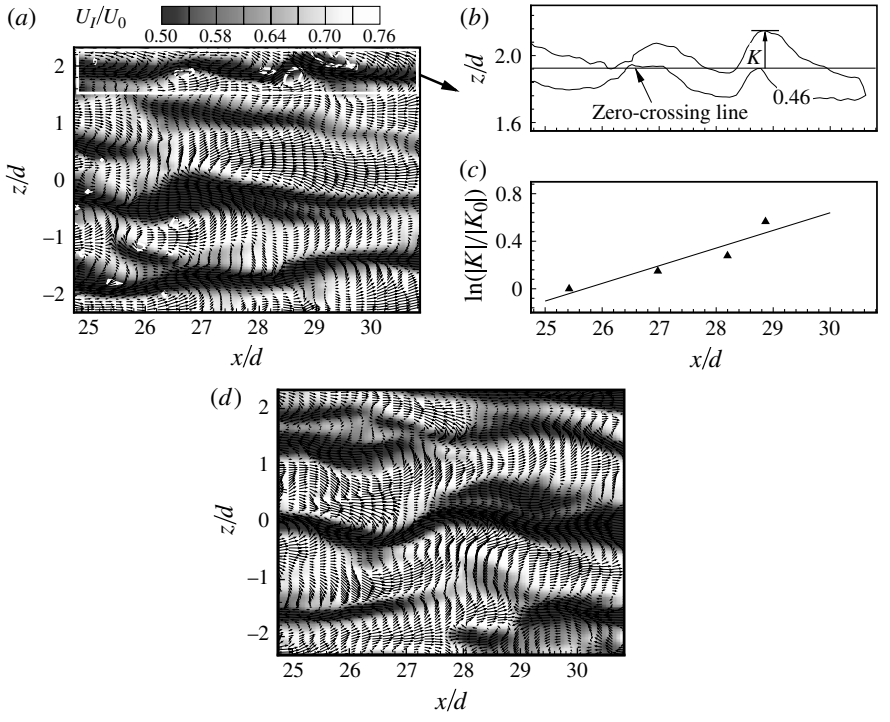


FIGURE 16. Instantaneous realizations depicting a spatially growing sinuous low-speed streak for the cylinder d_1 at $y_p/d = 3$ and for $Re_d = 1568$. Measurements at $x_1 = 250$ mm. Grey levels: normalized instantaneous velocity; vectors are fluctuating velocity vectors. (*a*) Spatially growing low-speed streak (see selected region). (*b*) Zoomed view of the selected streak in (*a*). (*c*) Spatial growth of the amplitude. (*d*) Oscillating streak in the process of generating new low-speed streaks.

strongly interact with each other in each cycle and cause horseshoe vortices to develop in a staggered array, as was also reported by Schlatter *et al.* (2008) from their simulation. However, defining the undulation amplitude, $|K|$, as the distance from the zero-crossing line of a wavy streak to its crest (see figure 16*b*), we find the growth of $|K|$ to be nearly exponential, as shown in figure 16(*c*); $|K_0|$ is the initial value of $|K|$. Such an exponential growth is noteworthy in wake-induced transition. Furthermore, Konishi & Asai (2010) find that the streak instability process in the nonlinear saturation stage generates wall-turbulent structures through the generation of new low-speed streaks (see their figure 10). A similar scenario may be seen in figure 16(*d*) even in the case of wake-induced transition.

3.4. *Secondary vortices and flow randomization*

A lifted-up shear layer, most likely to be associated with a Λ/hairpin vortex herein (as in figure 11*a*, for example), was often found to oscillate and shed several vortices, as shown in figure 17(*a*,*b*), for the cylinder d_1 at $y_p/d = 4$ and $Re_d = 1568$ case; vectors over grey levels are those viewed by an observer moving at a convection velocity, U_c, of vortices. Vortices are also identified by the swirling strength, λ_{ci} (line contours). The primary vortex, *P*, in the inclined shear layer is followed by several secondary vortices, *S*. It can also be seen that the spacing between two shed vortices does not change much with the downstream distance. Similar secondary vortices are also seen

https://doi.org/10.1017/jfm.2011.270 Published online by Cambridge University Press

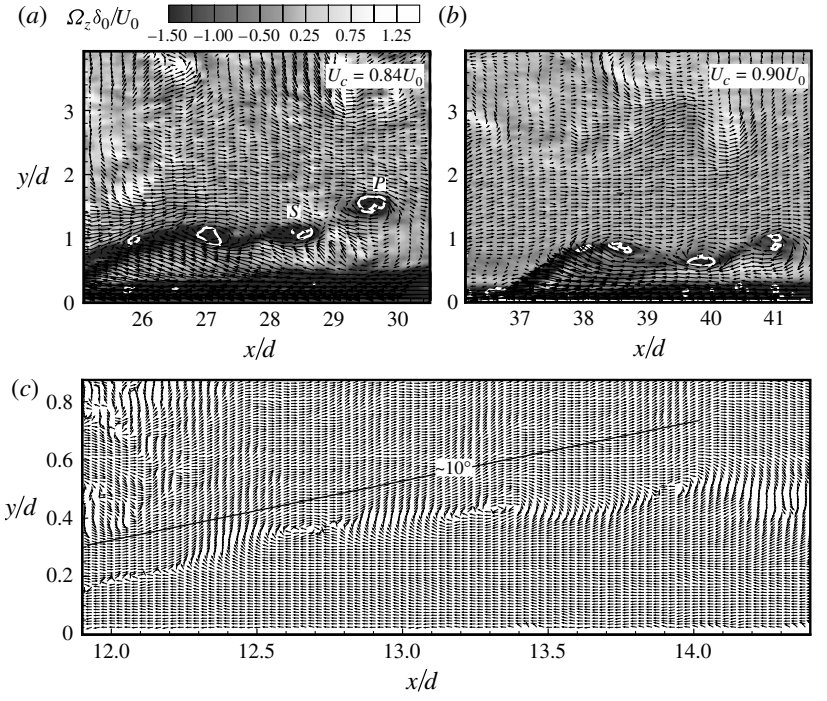


FIGURE 17. (*a*,*b*) Instantaneous secondary shedding in the wall-normal plane at $x_1 =$ 250 mm and 350 mm, respectively. Cylinder d_1 at $y_p/d = 4$ and $Re_d = 1568$ case. Grey levels are normalized instantaneous vorticity; contour line is the swirl strength, λ_{ci}; arrows are instantaneous velocity vectors viewed by an observer moving at U_c. (*c*) Conditional average showing imprint of shed vortices; cylinder d_2 at $y_p/d = 3$ and $Re_d = 1961$; $x_1 = 250$ mm; vectors scaled by their respective magnitude.

in several transitional flows (e.g. Reuter & Rempfer 2004; Pan *et al.* 2008; Durbin, Liu & Zaki 2009). Following Christensen & Adrian (2001), a conditional average of the fluctuating velocity field with a given $\lambda_{ci} > 0$ is estimated as

$$\langle v_j(\boldsymbol{x}')|\lambda_{ci}(\boldsymbol{x})\rangle \approx \frac{\langle \lambda_{ci}(\boldsymbol{x}) v_j(\boldsymbol{x}')\rangle}{\langle \lambda_{ci}(\boldsymbol{x})\lambda_{ci}(\boldsymbol{x})\rangle}\lambda_{ci}(\boldsymbol{x}). \tag{3.4}$$

This estimate reveals the statistical evidence of secondary vortices, as illustrated in figure 17(*c*) for the cylinder d_2 at $y_p/d = 3$ and $Re_d = 1961$; vectors are normalized by their magnitudes to show all the swirling motions clearly. It can be seen that almost equally spaced multiple vortices appear at an angle of approximately 10° to the flat plate. These multiple vortices seen here in a Galilean reference frame may be part of a hairpin packet usually seen in a turbulent boundary layer (e.g. Zhou *et al.* 1999).

Since the generation of several vortices from an inclined shear layer is important in the emergence of turbulence in a variety of flows (e.g. Nishioka, Asai & Iida 1981; Rist & Fasel 1995; Reuter & Rempfer 2004), it may be of interest to characterize the vortex shedding frequency. This is estimated from the spatial PIV data by following pairs of successive shed vortices (e.g. Svizher & Cohen 2006; Perret 2009). By separating those PIV realizations containing only the shed vortices from a hairpin vortex, we estimated the vortex shedding frequency as $f_h = U_c/\lambda$; λ is the distance between two shed vortices. The convection velocity, U_c, is considered to be constant

https://doi.org/10.1017/jfm.2011.270 Published online by Cambridge University Press

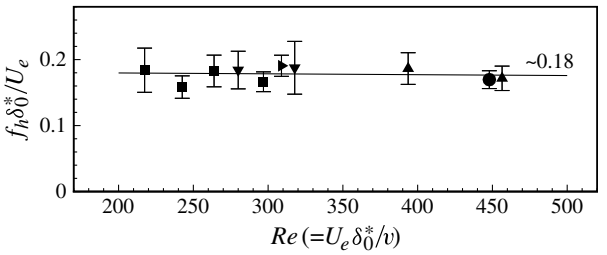


FIGURE 18. Vortex shedding frequency versus Reynolds number for both the cylinders: ■, d_1 at $y_p/d = 3$; ▲, d_1 at $y_p/d = 4$; ▼, d_2 at $y_p/d = 3$; ►, d_2 at $y_p/d = 3.25$; ●, d_2 at $y_p/d = 3.5$. Error bars indicate one standard deviation. Line is a fit to the data.

over λ; this is justified, as shed vortices in a particular frame maintain circular streamlines around the swirling strength contour while convecting at a particular U_c (see figure 17*a*,*b*, for example). We find that the normalized frequency, $f_h\delta_0^*/U_e$, so estimated is nearly independent of the flow Reynolds number ($Re_{\delta^*} = U_e\delta_0^*/\nu$) and the cylinder diameter, as shown in figure 18; the scatter may be attributed to the presence of a wake above the boundary layer, and the approximation made in estimating the frequency. This result is similar to that of Klebanoff, Tidstrom & Sargent (1962) in a controlled boundary layer transition. Although transition initiation can be different, some late-stage features may be expected to be similar but not yet explored fully. One such is the Reynolds number invariance of the vortex shedding frequency in both wake-induced and controlled boundary layer transitions.

While an inclined shear layer sheds negative vortices (clockwise), positive vortices (anticlockwise) were often seen to appear near the wall, along with clockwise vortices. This is elucidated in figure 19, for both the cylinders; fluctuating velocity vectors are shown over the spanwise vorticity contours (grey levels) and the swirling strength (line). These positive vortices were found to convect nearly at the local mean velocity. Thus, a positive vortex can be identified from fluctuations, as is also captured by the swirling strength contour (figure 19*a*,*b*). Similar structures with positive and negative vortices are also seen in the late stage of controlled boundary layer transition, with spikes between a pair of counter-rotating vortices due to the intersection of toroidal vortices in the x–y plane with the axis of symmetry in the streamwise direction (see Kachanov 1994, and his figure 31). Lee & Wu (2008) have reviewed several experimental results on boundary layer transition and find similar flow features even with different initial disturbance conditions. The Λ vortex, secondary vortex loops and the chain of ring vortices are of fundamental importance in understanding transitional wall-bounded flows. They also suggest that the interaction between a secondary vortex loop and a Λ vortex plays a key role in the generation of a high-frequency chain of ring vortices. From their simulation of controlled boundary layer transition, Rist & Fasel (1995) suggest that some vorticity lumps that are generated during the breakdown of the high-shear layer move towards the wall and merge with the region of high wall shear, while other vorticity lumps propagate away from the wall. Here, positive vortices associated with negative vortices resemble those of Rist & Fasel (1995). One may also notice that the fluctuating velocity vectors below the positive vortices in figure 19(*a*,*b*) show positive u fluctuations near the wall, and negative u fluctuations above these positive u fluctuations, along with detached vorticity. The maximum value of u/U_0 is about $\pm 30\,\%$, as can be seen in the u/U_0 contours in figure 19(*c*). These characteristics are seen in an incipient turbulent spot (Singer 1996)

https://doi.org/10.1017/jfm.2011.270 Published online by Cambridge University Press

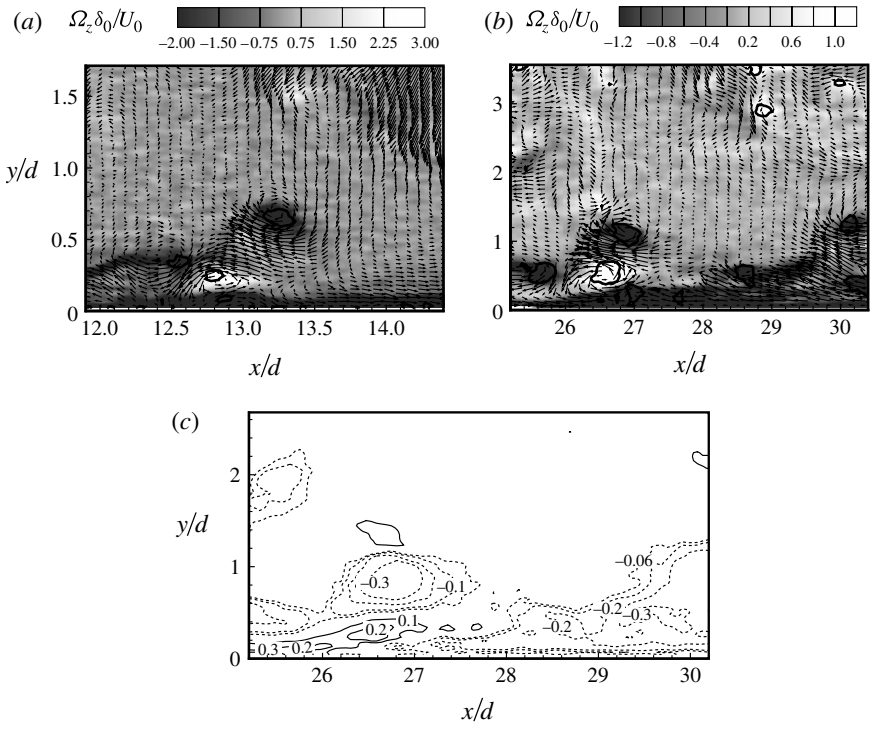


FIGURE 19. Instantaneous realizations depicting a positive vortex associated with a negative shed vortex at $x_1 = 250$ mm: (*a*) cylinder d_2 at $y_p/d = 3$, $Re_d = 1961$; and (*b*,*c*) cylinder d_1 at $y_p/d = 4$, $Re_d = 1568$. The u fluctuations in (*b*) are shown as contours of u/U_0 in (*c*). Arrows are fluctuating velocity vectors over the contour of normalized instantaneous vorticity.

and in bypass transition induced by free stream turbulence (Mandal *et al.* 2010). Therefore, the flow randomization is the same even in the case of a wake-induced boundary layer transition.

4. Discussion

The present study on wake-induced transition is mainly motivated by the reported differences between simulation (Ovchinnikov *et al.* 2006) and experimental (Pan *et al.* 2008) results. While Ovchinnikov *et al.* (2006) find some aspects of bypass transition in a wake-induced transition, Pan *et al.* (2008) suggest transition through the growth of hairpin structures generated due to the secondary instability of a spanwise vortex induced by a Kármán vortex street in the free stream.

Although the presence of spanwise vortices and hairpin-like structures observed by Pan *et al.* (2008) in their hydrogen bubble flow visualizations is confirmed here, several features of bypass transition are also seen in the present quantitative measurements. For example, the self-similarity of u_{rms} profiles in the initial growth phase, as reported by Ovchinnikov *et al.* (2006), and the linear energy growth are similar to those in bypass transition. Low- and high-speed streaks and their instability are the main features of bypass transition (e.g. Jacobs & Durbin 2001; Matsubara & Alfredsson 2001). Here, streaks are also observed in the late stages of wake-induced transition. While both varicose- and sinuous-like oscillations prevail in bypass

https://doi.org/10.1017/jfm.2011.270 Published online by Cambridge University Press

transition (e.g. Brandt, Schlatter & Henningson 2004; Mans *et al.* 2005; Mandal *et al.* 2010), the sinuous-like oscillation is seen to be more common in the present wake-induced transition case compared to only the varicose oscillation reported by Pan *et al.* (2008). The comparable wavelength of these oscillations ($\approx$(10–15)δ_0^*) with that in bypass transition (e.g. Schlatter *et al.* 2008) and the streak amplitude of about 35 % of the free stream speed in the late stage, similar to the streak instability results of Andersson *et al.* (2001) and Elofsson *et al.* (1999), support the streak feature in a wake-induced transition.

Transition through the generation of hairpin vortices in the late stage is generally seen in controlled boundary layer transition (e.g. Klebanoff *et al.* 1962; Bake *et al.* 2000). Pan *et al.* (2008) suggest a similar transition process even in the case of a wake-induced transition, as is also seen in the present study (see figures 17 and 19). However, the present study also reveals the possibility of a streak secondary instability process (see figure 16), as in bypass transition induced by free stream turbulence (e.g. Schlatter *et al.* 2008). The existence of both these transition scenarios is also reported for other transitional flows (e.g. Brandt *et al.* 2004; Gavarini, Bottaro & Nieuwstad 2004). The experimental study on the boundary layer transition in a concave wall by Swearingen & Blackwelder (1987) also suggests the simultaneous existence of both the hairpin vortex mode and the lateral sinuous mode transition (see their figure 14).

5. Summary

Wake-induced boundary layer transition has been investigated using the PIV technique. In the early stage, wake induces spanwise vortices, which subsequently generate Λ structures (hairpin vortices), as reported by Pan *et al.* (2008). The physical size of these structures depends on the Reynolds number, Re_d, and the upstream position of the wake generating cylinder, as is also substantiated by some statistical analysis of the data. In the spanwise plane, these Λ vortices appear in a somewhat staggered manner. The quasi-subharmonic peak at about half the Strouhal frequency of the cylinder wake (in the power spectrum of the hot-wire signal), as was also reported by Pan *et al.* (2008), may be responsible for this staggered arrangement.

The self-similar u_{rms} profiles and the rapid linear energy growth suggest that even a wake-induced transition may undergo algebraic growth at some stage of disturbance development (most likely, while spanwise vortices deform to create hairpin vortices and streaks). Inclined shear layers, typical in transition, are found to be associated with a pattern of negative streamwise velocity fluctuations and a vortical structure atop the shear layer indicating the lifted-up hairpin structure (e.g. Adrian *et al.* 2000). Positive u fluctuations, which are associated with high-velocity regions, appear along with high-shear layers near the wall. By conditional averaging of these positive and negative u fluctuations, it is shown that the peak u_{rms} movement towards the wall is due to positive u fluctuations. Also, the total u_{rms} can be represented reasonably well by a linear combination of the respective r.m.s. of positive and negative u fluctuations.

Streamwise velocity streaks with an average spanwise spacing comparable to the simulation results of Ovchinnikov *et al.* (2006) undergo oscillations more like the sinuous type. Irrespective of the cylinder size and location, the streak amplitude is found to saturate at $\sim$35 % of the free stream speed. According to controlled studies (Elofsson *et al.* 1999; Andersson *et al.* 2001), secondary instability on streak may set in at such an amplitude. Interestingly, the undulation amplitude of some sinuous streaks exhibits nearly exponential growth, which indicates that a secondary instability process may play an important role in the streak breakdown process.

https://doi.org/10.1017/jfm.2011.270 Published online by Cambridge University Press

A hairpin vortex while growing downstream sheds vortices. The normalized shedding frequency of these vortices is shown here to be independent of the Reynolds number ($U_e\delta_0^*/\nu$), similar to that inferred by Klebanoff *et al.* (1962) in controlled boundary layer transition. While a hairpin sheds vortices, a negative shed vortex (clockwise) is often accompanied by a positive vortex (anticlockwise) having convection velocity nearly equal to the local mean flow velocity. It is suggested that this process contributes to the flow randomization, as was also seen in bypass transition induced by free stream turbulence (Mandal *et al.* 2010).

On the whole, though they have both similar and dissimilar events, the late-stage process seems to be the same in wake-induced boundary layer transition and bypass transition. Also, a wake-induced boundary layer transition seems to undergo breakdown via the appearance of a hairpin vortex, which shed vortices, and streak instability process, as well.

The authors wish to thank the Department of Science and Technology for funding the PIV unit. We are grateful to Professor R. Goverdhan and his students, Mr Pankaj and Mr Jayaprakash, of the Mechanical Engineering Department for lending us their laser at a time of crisis. We sincerely thank Mr Manu for his help during this study, and Mr A. Ghatak for his linguistic help. We also thank the referees for their comments and suggestions.

REFERENCES

ACARLAR, M. S. & SMITH, C. R. 1987 A study of hairpin vortices in a laminar boundary layer. Part 1. Hairpin vortices generated by a hemisphere protuberance. *J. Fluid Mech.* **175**, 1–41.

ADRIAN, R. J. 2007 Conditional averages and stochastic estimation. In *Handbook of Experimental Fluid Mechanics* (ed. A. L. Yarin, C. Tropea & J. F. Foss), pp. 1370–1378. Springer.

ADRIAN, R. J., MEINHART, C. D. & TOMKINS, C. D. 2000 Vortex organization in the outer region of the turbulent boundary layer. *J. Fluid Mech.* **422**, 1–54.

ANDERSSON, P., BRANDT, L., BOTTARO, A. & HENNINGSON, D. 2001 On the breakdown of boundary layer streaks. *J. Fluid Mech.* **428**, 29–60.

ANGRILL, F., BERGAMASCHI, S. & COSSALTER, V. 1982 Investigation of wall induced modifications to vortex shedding from a circular cylinder. *Trans. ASME: J. Fluids Engng* **104**, 518–522.

BAKE, S., FERNHOLZ, H. H. & KACHANOV, Y. S. 2000 Resemblance of k- and n-regimes of boundary-layer transition at late stages. *Eur. J. Mech.* B/*Fluids* **19**, 1–22.

BANERJEE, A. S., MANDAL, A. C. & DEY, J. 2006 Particle image velocimetry studies of an incipient spot in the Blasius boundary layer. *Exp. Fluids* **40**, 928–941.

BRANDT, L. & HENNINGSON, D. S. 2002 Transition of streamwise streaks in zero-pressure-gradient boundary layers. *J. Fluid Mech.* **472**, 229–261.

BRANDT, L., SCHLATTER, P. & HENNINGSON, D. S. 2004 Transition in boundary layers subject to free-stream turbulence. *J. Fluid Mech.* **517**, 167–198.

CHRISTENSEN, K. T. & ADRIAN, R. J. 2001 Statistical evidence of hairpin vortex packets in wall turbulence. *J. Fluid Mech.* **431**, 433–443.

DOLIGALSKI, T. L., SMITH, C. R. & WALKER, J. D. A. 1994 Vortex interactions with walls. *Annu. Rev. Fluid Mech.* **26**, 573–616.

DOLIGALSKI, T. L. & WALKER, J. D. A. 1984 The boundary layer induced by a convected two-dimensional vortex. *J. Fluid Mech.* **139**, 1–28.

DURBIN, P. A., LIU, Y. & ZAKI, T. A. 2009 Interaction of discrete and continuous boundary layer modes to cause transition. *Intl J. Heat Fluid Flow* **30**, 403–410.

ELOFSSON, P. A. & ALFREDSSON, P. H. 1998 An experimental study of oblique transition in plane Poiseuille flow. *J. Fluid Mech.* **358**, 177–202.

https://doi.org/10.1017/jfm.2011.270 Published online by Cambridge University Press

ELOFSSON, P. A., KAWAKAMI, M. & ALFREDSSON, P. H. 1999 Experiments on the stability of streamwise streaks in plane Poiseuille flow. *Phys. Fluids* **11**, 915–930.

FRANSSON, J. H. M., MATSUBARA, M. & ALFREDSSON, P. H. 2005 Transition induced by freestream turbulence. *J. Fluid Mech.* **527**, 1–25.

GAD-EL-HAK, M., DAVIS, S. H., MCMURRAY, J. T. & ORSZAG, S. A. 1984 On the stability of the decelerating laminar boundary layer. *J. Fluid Mech.* **138**, 297–323.

GAVARINI, M. I., BOTTARO, A. & NIEUWSTAD, F. T. M. 2004 The initial stage of transition in pipe flow: role of optimal base-flow distortions. *J. Fluid Mech.* **517**, 131–165.

JACOBS, R. G. & DURBIN, P. A. 2001 Simulations of bypass transition. *J. Fluid Mech.* **428**, 185–212.

KACHANOV, Y. S. 1994 Physical mechanism of laminar-boundary-layer transition. *Annu. Rev. Fluid Mech.* **26**, 411–482.

KLEBANOFF, P. S., TIDSTROM, K. D. & SARGENT, L. M. 1962 The three dimensional nature of boundary-layer instability. *J. Fluid Mech.* **12**, 1–34.

KONISHI, Y. & ASAI, M. 2010 Development of subharmonic disturbance in spanwise-periodic low-speed streaks. *Fluid Dyn. Res.* **42**, 035504.

KOSTAS, J., SORIA, J. & CHONG, M. S. 2002 Particle image velocimetry measurements of a backward-facing step flow. *Exp. Fluids* **33**, 838–853.

KYRIAKIDES, N. K., KASTRINAKIS, E. G., NYCHAS, S. G. & GOULAS, A. 1996 Boundary layer transition induced by a von Karman vortex street wake. *Proc. Inst. Mech. Engrs* **12**, 167–179.

KYRIAKIDES, N. K., KASTRINAKIS, E. G., NYCHAS, S. G. & GOULAS, A. 1999 Aspects of flow structure during a cylinder wake-induced laminar/turbulent transition. *AIAA J.* **37**, 1197–1205.

LEE, C. B. & WU, J. Z. 2008 Transition in wall-bounded flows. *Appl. Mech. Rev.* **61**, 030802.

LIU, X. & RODI, W. 1991 Experiments on transitional boundary layers with wake-induced unsteadiness. *J. Fluid Mech.* **231**, 229–256.

LIU, Y., ZAKI, T. A. & DURBIN, P. A. 2008 Boundary-layer transition by interaction of discrete and continuous modes. *J. Fluid Mech.* **604**, 199–233.

LOURENCO, L. M. & KROTHAPALLI, A. 2000 TRUE resolution PIV: a mesh-free second order accurate algorithm. In *Proceedings of the International Conference in Applications of Lasers to Fluid Mechanics, Lisbon, Portugal*.

LUCHINI, P. 2000 Reynolds-number-independent instability of the boundary layer over a flat surface: optimal perturbations. *J. Fluid Mech.* **404**, 289–309.

MANDAL, A. C. 2010 A study on boundary layer transition induced by large freestream disturbances. PhD thesis, Indian Institute of Science, Bangalore, India.

MANDAL, A. C., VENKATAKRISHNAN, L. & DEY, J. 2010 A study on boundary layer transition induced by freestream turbulence. *J. Fluid Mech.* **660**, 114–146.

MANS, J., KADIJK, E. C., DE LANGE, H. C. & VAN STEENHOVEN, A. A. 2005 Breakdown in a boundary layer exposed to free-stream turbulence. *Exp. Fluids* **39**, 1071–1083.

MANS, J., DE LANGE, H. C. & VAN STEENHOVEN, A. A. 2007 Sinuous breakdown in a flat plate boundary layer exposed to free-stream turbulence. *Phys. Fluids* **19**, 088101.

MATSUBARA, M. & ALFREDSSON, P. H. 2001 Disturbance growth in boundary layers subjected to free-stream turbulence. *J. Fluid Mech.* **430**, 149–169.

MAYLE, R. E. 1991 The role of laminar–turbulent transition in gas turbine engines. *Trans. ASME: J. Turbomach.* **113**, 509–537.

MORKOVIN, M. V. 1969 The many faces of transition. In *Viscous Drag Reduction* (ed. C. S. Wells). Plenum.

NARASIMHA, R., DEVASIA, K. J., GURURANI, G. & BADRI NARAYANAN, M. A. 1984 Transitional intermittency in boundary layers subjected to pressure gradient. *Exp. Fluids* **2**, 171–176.

NARASIMHA, R. & PRASAD, S. N. 1994 Leading edge shape for flat plate boundary layer studies. *Exp. Fluids* **17**, 358–360.

NISHIOKA, M., ASAI, M. & IIDA, S. 1981 Wall phenomena in the final stage of transition to turbulence. In *Transition and Turbulence* (ed. R. E. Meyer), pp. 113–126. Academic.

https://doi.org/10.1017/jfm.2011.270 Published online by Cambridge University Press

ONG, L. & WALLACE, J. 1996 The velocity field of the turbulent very near wake of a circular cylinder. *Exp. Fluids* **20**, 441–453.

OVCHINNIKOV, V., CHOUDHARI, M. M. & PIOMELLI, U. 2008 Numerical simulations of boundary-layer bypass transition due to high-amplitude free-stream turbulence. *J. Fluid Mech.* **613**, 135–169.

OVCHINNIKOV, V., PIOMELLI, U. & CHOUDHARI, M. M. 2006 Numerical simulations of boundary-layer transition induced by a cylinder wake. *J. Fluid Mech.* **547**, 413–441.

PAN, C., WANG, J. J., ZHANG, P. F. & FENG, L. H. 2008 Coherent structures in bypass transition induced by a cylinder wake. *J. Fluid Mech.* **603**, 367–389.

PELLERIN, S. & GIOVANNINI, A. 1999 Interaction vortex – boundary layer: numerical study of wall mechanisms. *ESAIM: Proc.* **7**, 325–334.

PERRET, L. 2009 PIV investigation of the shear layer vortices in the near wake of a circular cylinder. *Exp. Fluids* **47**, 789–800.

PRICE, S. J., SUMNER, D., SMITH, J. G., LEONG, K. & PAIGDOUSSIS, M. P. 2002 Flow visualization around a circular cylinder near to a plane wall. *J. Fluids Struct.* **16**, 175–191.

REUTER, J. & REMPFER, D. 2004 Analysis of pipe flow transition. Part I. Direct numerical simulation. *Theor. Comput. Fluid Dyn.* **17**, 273–292.

RIST, U. & FASEL, H. 1995 Direct numerical simulation of controlled transition in a flat-plate boundary layer. *J. Fluid Mech.* **298**, 211–248.

SARKAR, S. & SARKAR, S. 2009 Large-eddy simulation of wake and boundary layer interactions behind a circular cylinder. *Trans. ASME: J. Fluids Engng* **131**, 091201.

SAVILL, A. & ZHOU, M. 1983 Wake/boundary layer and wake/wake interactions–smoke flow visualization and modeling. In *Proc. 2nd Asian Congress of Fluid Mechanics* (ed. M. C. Ko), pp. 743–754. Science Press.

SCHLATTER, P., BRANDT, L., DE LANGE, H. C. & HENNINGSON, D. S. 2008 On streak breakdown in bypass transition. *Phys. Fluids* **20**, 101505.

SCHRÖDER, A. 2001 Untersuchung der Strukturen von künstlich angeregten transitionellen Plattengrenzschichtströmungen mit Hilfe der Stereo und Multiplane Particle Image Velocimetry. PhD thesis, University of Göttingen, Germany. http://webdoc.sub.gwdg.de/diss/2001/schroeder/schroeder.pdf.

SINGER, B. A. 1996 Characteristics of a young turbulent spot. *Phys. Fluids* **8**, 509–521.

SQUIRE, L. C. 1989 Interactions between wakes and boundary layers. *Prog. Aerosp. Sci.* **26**, 261–288.

SVIZHER, A. & COHEN, J. 2006 Holographic particle image velocimetry measurements of hairpin vortices in subcritical air channel flow. *Phys. Fluids* **18**, 014105.

SWEARINGEN, J. D. & BLACKWELDER, R. F. 1987 The growth and breakdown of streamwise vortices in the presence of a wall. *J. Fluid Mech.* **182**, 255–290.

TOMKINS, C. D. & ADRIAN, R. J. 2003 Spanwise structure and scale growth in turbulent boundary layers. *J. Fluid Mech.* **490**, 37–74.

WESTIN, K. J. A., BOIKO, A. V., KLINGMANN, B. G. G., KOZLOV, V. V. & ALFREDSSON, P. H. 1994 Experiments in a boundary layer subjected to free stream turbulence. Part 1. Boundary layer structure and receptivity. *J. Fluid Mech.* **281**, 193–218.

ZHOU, J., ADRIAN, R. J., BALACHANDAR, S. & KENDALL, T. M. 1999 Mechanism for generating coherent packets of hairpin vortices in channel flow. *J. Fluid Mech.* **387**, 353–396.

ZHOU, M. D. & SQUIRE, L. C. 1985 The interaction of a wake with a turbulent boundary-layer. *J. Aeronaut.* **89**, 72–81.

https://doi.org/10.1017/jfm.2011.270 Published online by Cambridge University Press